

# An HVS-Oriented Saliency Map Prediction Modeling

Qiang Li

Image and Signal Processing Lab, University of Valencia, 46980, Spain

qiang.li@uv.es

**Abstract.** Visual attention is one of the most significant characteristics for selecting and understanding the outside world. The nature complex scenes, including larger redundancy and human vision, can't be processing all information simultaneously because of the information bottleneck. The visual system mainly focuses on dominant parts of the scenes to reduce the input visual redundancy information. It's commonly known as visual attention prediction or visual saliency map. This paper proposes a new saliency prediction architecture inspired by human low-level visual cortex function. The model considered the opponent color channel, wavelet energy map, and contrast sensitivity function for extract image features and maximum approach to real visual neural network function in the brain. The proposed model is evaluated several datasets, including MIT1003<sup>1</sup>, MIT300<sup>2</sup>, TORONTO<sup>3</sup>, and SID4VAM<sup>4</sup> to explain its efficiency. The proposed model results are quantitatively and qualitatively compared to other state-of-the-art salience prediction models and their achieved slightly outperforms of visual saliency prediction.

**Keywords:** visual saliency · redundancy · low-level visual cortex · opponent color channel · contrast sensitivity function · wavelet energy map

## 1 Introduction

Visual attention or selection is one of the significant features in the Human Vision System (HVS) to drive compact information from the complex nature scenes [Treisman and Gelade, 1980]. The nature scene images, including amount redundancy and usually useless for scene categories or recognition and vision attention mechanism, can extract essential features from redundant data, which

<sup>1</sup> <http://people.csail.mit.edu/tjudd/WherePeopleLook/index.html>

<sup>2</sup> <http://saliency.mit.edu/>

<sup>3</sup> <http://www-sop.inria.fr/members/Neil.Bruce/>

<sup>4</sup> [http://www.cvc.uab.es/neurobit/?page\\_id=53](http://www.cvc.uab.es/neurobit/?page_id=53)

benefit visual information processing efficiency in the brain. The phenomenon of visual attention has been studied for a long time [Sun and Fisher, 2003]. According to Barlow’s *Efficiency Coding Hypothesis*, visual attention can be used to explain the Barlow’s theory, and it has used to select relevant information and remove irrelevant information from redundant vision scenes [Barlow, 1959]. Furthermore, vision saliency has already become a hot research topic spanning neuroscience and computer vision disciplines. In general, there are two types of visual attention mechanisms: bottom-up and top-down branches. Bottom-up models are mainly stimulus-driven, and it is used to extract image features along with visual information processing in the brain, e.g., color, frequency, texture, orientation, and motion [Wang et al., 2005]. In contrast, the top-down approach, which is goal-driven, is usually high-level cognitive feedback and modulates low-level vision functional at a specific level [Itti, 2000]. Both computational neural modeling has been achieved application successfully in the saliency map prediction.

Many studies have tried to estimate bottom-up or top-down computational modeling to predict the saliency map. One of the earliest classical computational modelings is based on bottom-up mechanisms proposed by Itti *et al.* [Itti et al., 1998]. The model estimates the saliency map based on a human low-level vision system that extracts low-level image features, e.g., color, orientation, and intensity conspicuity map. The model structure can be defined as: input image  $\rightarrow$  linear filtering (colors, intensity, orientations)  $\rightarrow$  center-surround differences and normalization  $\rightarrow$  across-scale combinations and normalization  $\rightarrow$  linear combinations  $\rightarrow$  saliency map. The model achieved a good result in the saliency prediction. Furthermore, in the last few years, some studies have tried to estimate the saliency map with deep convolutions neural networks (CNNs), and they have achieved impressive performances compared to conventional methods [Kruthiventi et al., 2016]. Compared to conventional methods, deep learning implantation easier to transfer to real-life applications, such as object detection, object recognition, scene classification, video understanding, and image compression.

Recently, wavelet transform (WT) also have begun to be used to estimate the computational vision saliency map [Murray et al., 2011]. Compared to the Fourier Transform, it has a high resolution in both the frequency- and the time-domain. WT can decompose signals on different scales is also known as multi-resolution/multi-scale analysis, or called sub-band coding that captures more low-level features from the original signal [Louis et al., 1997]. Furthermore, the WT approach can explain the primary visual cortex (V1) properties and produced multi-scale and multi-orientation features when given stimulus. The final saliency map estimate with a sum up all the processed wavelet coefficients then inverse WT (IWT) [Selvaraj and Shebiah, 2009]. The shortcomings of WT estimate saliency map loss of global contract information rather than local contrast information. However, wavelet energy (WE) maps have barely been considered in the saliency map estimation. Therefore, we implemented WE into proposed computational modeling.

In this study, we proposed a human low-level vision cortex inspired saliency predication framework. The model first introducing the contrast sensivity function and wavelet energy into model to predict human visual attention in the field of view. The proposed model is stimuli-driven model or bottom-up model and it evaluate with certain metrics e.g. Area under ROC curve (AUC) [Borji et al., 2013], Normalized Scanpath Saliency (NSS) [Emami and Hoberock, 2013], Pearson’s Correlation Coefficient (CC) [Engelke et al., 2012], Similarity or histogram intersection (SIM) [Riche et al., 2013], Kullback-Leibler divergence (KL) [Wilming et al., 2011], and Information Gain (IG) [Kümmerer et al., 2015]. The details of above metrics will introduce in the section 3. The proposed model was quantitatively evaluated with MIT1003 and SID4VAM datasets compared with other different models.

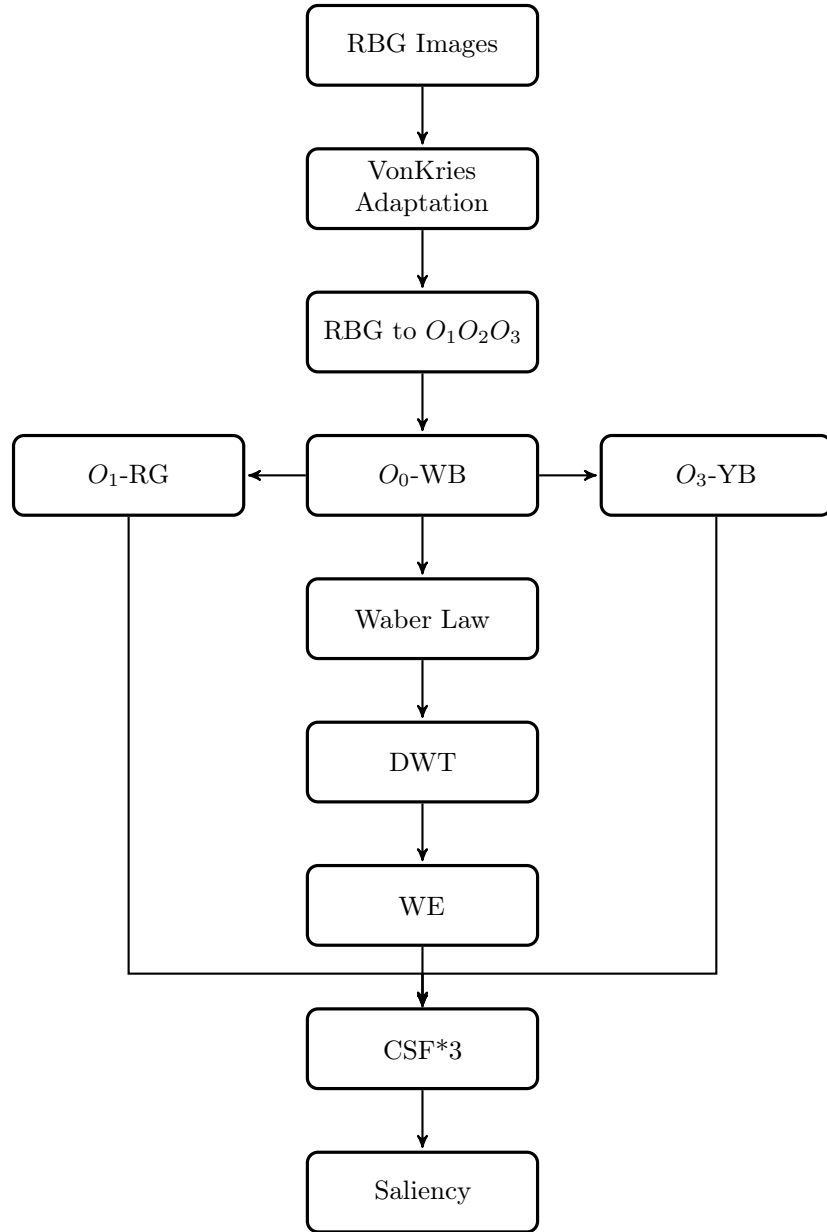
Saliency Prediction Modeling References			
Model	Authors	Year	Inspiration
ITII	[Itti et al., 1998]	1998	Biological
Achanta	[Achanta et al., 2009]	2009	Fourier/Spectral
AIM	[Bruce and Tsotsos, 2005]	2005	Biological/Information-Theoretic
HFT	[li et al., 2012]	2013	Fourier/Spectral
ICL	[Hou and Zhang, 2008]	2008	Information-Theoretic/Probabilistic
SIM	[Murray et al., 2011]	2011	Biological

The rest of this paper is organization as follows: Section II introduce the concept opponent color space, wavelet decomposition and wavelet energy map estimation and contrast sensitivity functional, then present the details of model structure. Section III introduced the model predict saliency map with different datasets and the details of evaluate metric from mathematics views. Section IV introduce introduce the experiment results. The final section gives conclusions for the paper.

## 2 The Proposed Saliency Prediction Model

### 2.1 Saliency Prediction Model

The biological like visual saliency prediction map is proposed spired by the human low-level visual system. The information flow, along with the retina, LGN, and V1, is the fundamental component of the optical neural network. The proposed model’s architecture mainly contained color opponent channel, wavelet transform, and contrast sensitivity function. The color opponent channel simulates the retina cells to respond to different spectral wavelengths, and wavelet transform mainly simulates the V1 multi-scale, multi-orientation properties. The CSF mainly simulates the human brain’s susceptible to spatial frequency. The details of each component will be described in the following sections, respectively. The computational saliency prediction model architecture is illustrated as follows:



In the next subsection, we will introduce three significant parts in the above model: color opponent space, DWT/WE, and CSF, respectively.

## 2.2 Color Appearance Model

In this section, we describe the color appearance space component in the proposed model. Color representation in the brain can significantly improve object

recognition, identity and reduce redundancy; as we said before, visual information input from the natural environment includes heavy redundancy [Barlow, 1990]. The Trichromatic Theory [Brill, 2014] and the color appearance model proposed, which is inspired by low-level human visual system function, helps us understand how the sensors encode color information and widely used in low-level image processing and feature extraction. The two functional types of chromatic sensitivity or selectivity sensors were found: Single-Opponent and Double-Opponent neurons based on long (L), mediate (M), short (S) cones response in the physical world [Shapley and Hawken, 2011] (see Fig.1).

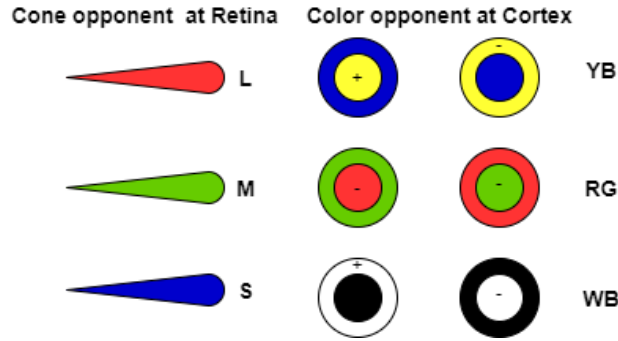


**Fig. 1.** The receptive field of opponent color space "+" indicate excitation, "-" represent inhibition.

The most saliency predicts model used opponent color space is CIE Lab and YUV color space. In our case, we were introducing a new opponent color space proposed by Hering [Hurvich and Jameson, 1957]. The color space from RGB to  $O_1O_2O_3$  transform matrix can be defined as:

$$\begin{bmatrix} O_1 \\ O_2 \\ O_3 \end{bmatrix} = \begin{bmatrix} 0.2814 & 0.6938 & 0.0638 \\ -0.0971 & 0.1458 & -0.0250 \\ -0.0930 & -0.2529 & 0.4665 \end{bmatrix} \begin{bmatrix} sR \\ sG \\ sB \end{bmatrix} \quad (1)$$

The test nature RGB scene images (size are 256x256, 512x512) selected from Signal and Image Processing Institute, University of Southern California <sup>5</sup> and Kodak lossless true color image database <sup>6</sup>(size are 512x768, 768x512, 768x512). The total nature color images are resized into the same size (8 bits, 256x256) as test images (see Fig.2).

<sup>5</sup> <http://sipi.usc.edu/database/database.php?volume=misc>

<sup>6</sup> <http://r0k.us/graphics/kodak/>

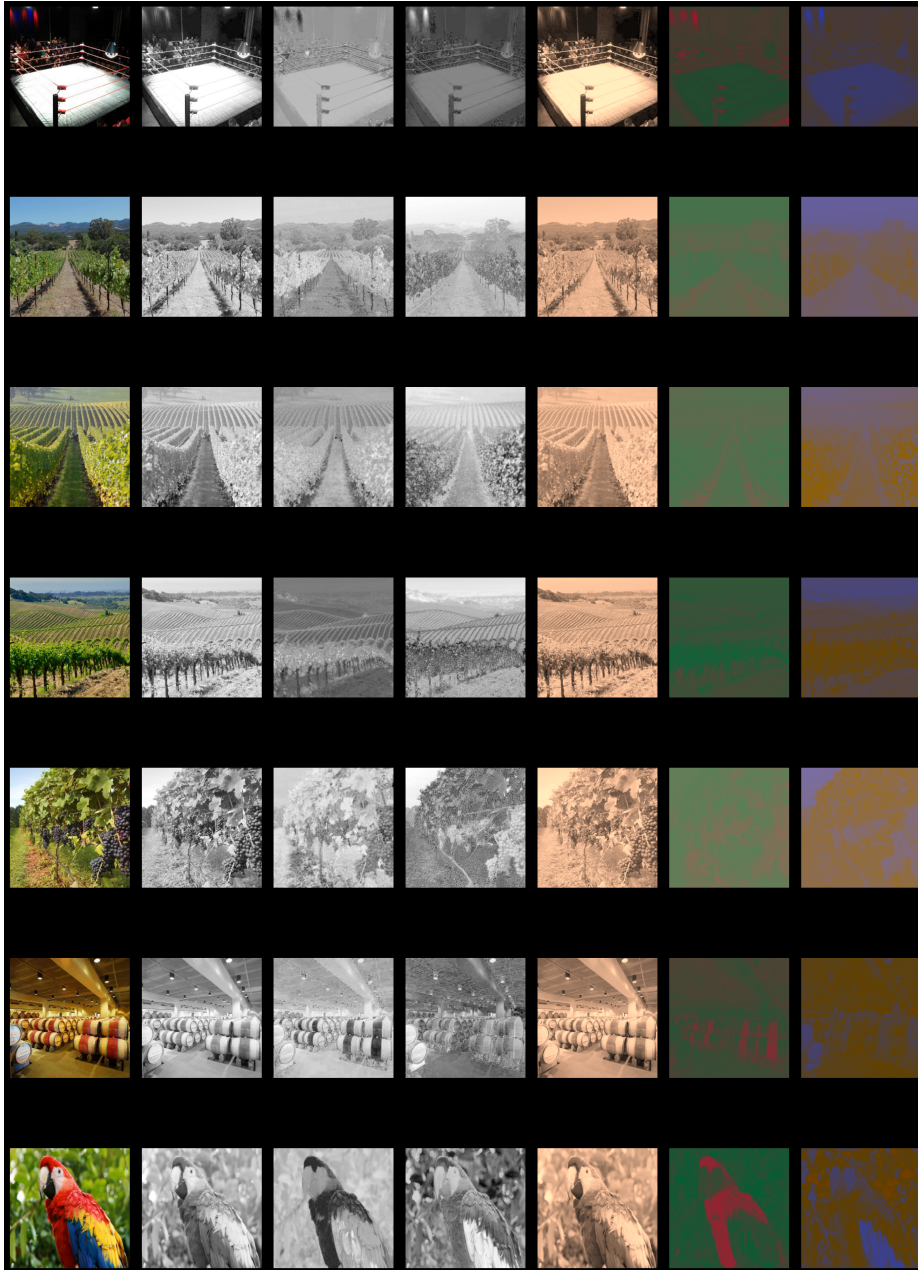


**Fig. 2.** Color opponent processing. The first column denotes raw RGB color space, then follow the White-Black (WB) channel, Red-Green (RG) channel, and Yellow-Blue (YB) channel with a gray colormap, respectively. The last three columns also represent the WB, RG, and YB channels and artificial color for better visualization of opponent processing at the visual cortex level.

### 2.3 Wavelet Energy Map

The wavelet image analysis can be decomposed image into multi-scale and multi-orientation features similar to visual cortex representation. Compared to the Fourier Transform (FT), WT can represent spatial and frequency information simultaneously. WT approach firstly proposed by Alferd Haar, and it has already been widely used in signal analysis, e.g., image compression, image de-noising, classification, etc. WT was already applied in the visual saliency map prediction and achieved good performance [imamoğlu et al., 2013]. However, WE are still barely used in the visual saliency map prediction, and it can be used to enhance local contrast information in the decomposition sub-bands. Discrete Wavelet Transform (DWT) used in our proposed model and its basic principle can be mathematically expressed as:

$$r[n] = ((I * f)[n]) \downarrow 2 = \left( \sum_{k=-\infty}^{\infty} I[k]f[n - k] \right) \downarrow 2 \quad (2)$$

Where  $I$  indicates input images,  $f$  represents a series of filter banks (low-pass and high-pass), and  $\downarrow 2$  indicates down-sampling until the next layer signal cannot be decomposed any more. A series of sub-band images are produced after convolution with DWT, and then WE can be calculated from each sub-band features (see Fig.3).

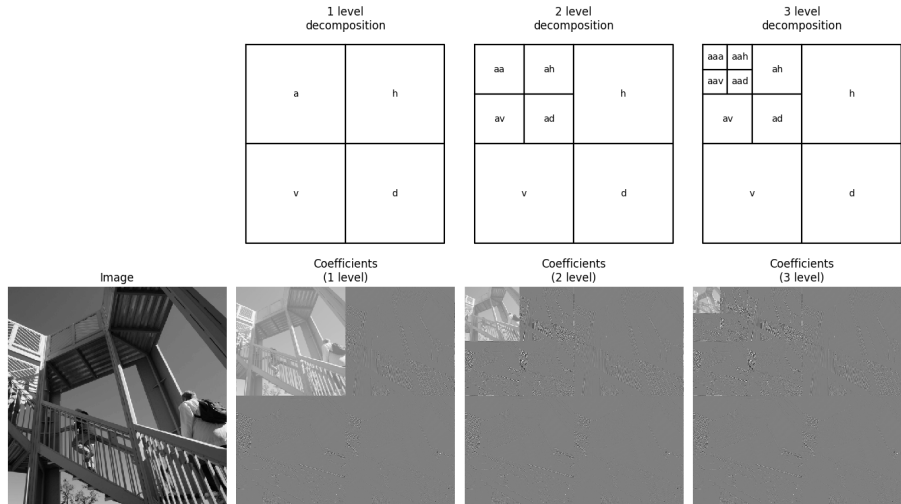


**Fig. 3.** The different decomposition level with DWT

The wavelet energy map can be expressed as:

$$\mathcal{WE}(i, j) = \|I(i, j)\|^2 = \sum_{k=1}^{3ind+1} |I_k(i, j)|^2 \quad (3)$$

Where *ind* indicates the maximum level of an image can be decomposed in the last, and  $I_k(i, j)^2$  represents the energy map of each sub-band features (see Fig.3 and Fig.4).

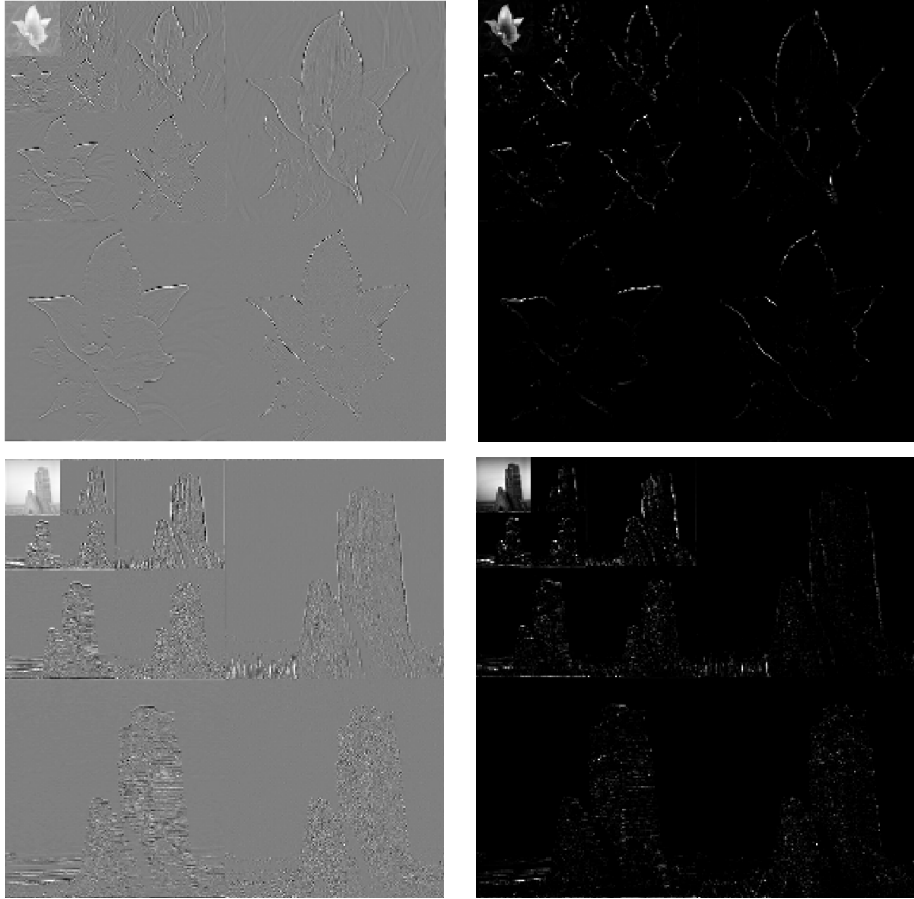


**Fig. 4.** DWT and WE map

The visual simple and complex cells can be modeled by wavelet. In our case, we are not considered more details of each hyper-column neuron interactions

(e.g., Li's model [Zhaoping, 1998]). The V1 complex cell can sum all square of different scales and orientations (see Fig.5).

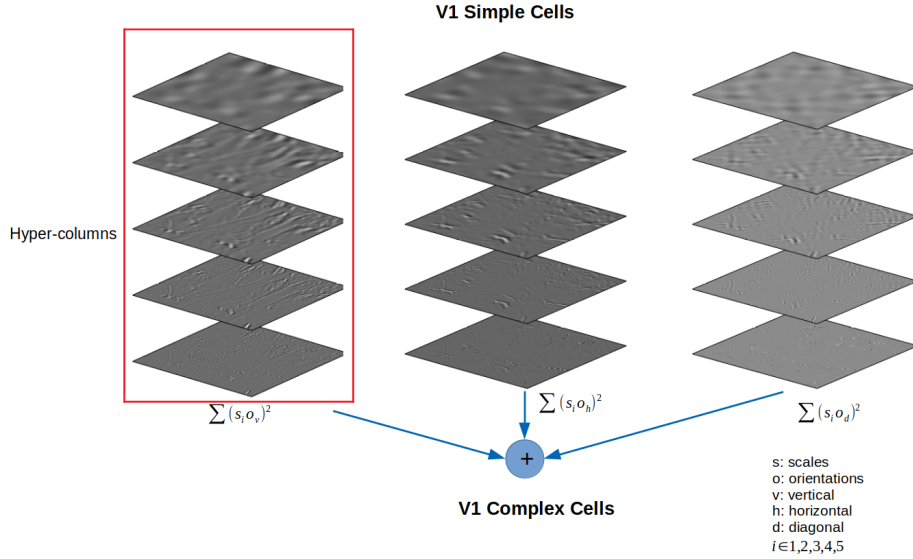


**Fig. 5.** V1 simple and complex cells modeling

## 2.4 Contrast Sensivity Function

The human visual system is compassionate of contrast change in the natural environment. The visual cortex can decompose the complex signal into sub-band compositions, and one of the significant features is CSF. It can be divided into achromatic and chromatic spatial CSFs [Mullen, 1985]. In this proposed computational modeling, achromatic CSF was implemented into the model, which was firstly proposed by Mannos and Sakrison in 1974 [Mannos and Sakrison, 1974]. The achromatic CSF mathematics can be expressed as:

$$H_{\text{CSF}}(f, \theta) = H_1(f, \theta)H_2(f, \theta) \quad (4)$$

where  $f$  is radial frequency in cycles/degree, and  $\theta \in [-\pi, \pi]$  denotes the angular frequency.  $H_1(f, \theta)$  is the frequency response of a circularly symmetric Gaussian filter and  $H_2(f, \theta)$  is the frequency response of a CSF model originally proposed by Mannos and Sakrison [Mullen, 1985] and adjusted by Daly [Daly, 1992].  $H_1$ ,  $H_2$  can be formula expressed as:

$$H_1(f, \theta) = \exp(-2\pi^2\sigma^2 f^2) \quad (5)$$

$$H_2(f, \theta) = \begin{cases} 2.6 (0.0192 + \lambda f_0) \exp[-\lambda f_\theta], & f \geq f_{\text{peak}} \\ 0.981, & \text{otherwise} \end{cases} \quad (6)$$

Where  $\lambda = 0.114$ ,  $f_\theta = \frac{f}{0.15 \cos(4\theta) + 0.85}$  accounts for the oblique effect, in other words,  $f_\theta$  represents an orientation-based modification of  $f$  which leads to a decrease in the contrast sensitivity along with diagonal orientations (see Fig.6).

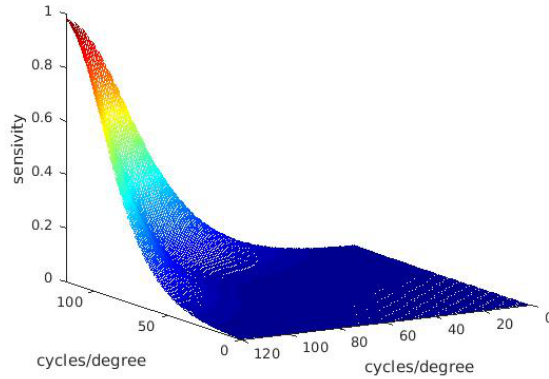


**Fig. 6.** Spatial representation of contrast sensitivity functions.

### 3 Materials and Methods

#### 3.1 Datasets

The proposed model was evaluated on several well-known datasets, including MIT1003, MIT 300, TORONTO and SID4VAM, which are described below.

**MIT1003** MIT1003 is an image dataset that includes 1003 images from the Flickr and LabelMe collections (see Fig.7). The fixation map was generated from recording 15 participants' eye-tracking data. It is the largest eye tracking dataset. The dataset includes 779 landscapes and 228 portraits images spanning size from  $405 \times 405$  to  $1024 \times 1024$  pixels [Judd et al., 2012].

**MIT300** MIT300 is a benchmark saliency test dataset that includes 300 images from recoding 39 observers' eye-tracking dataset. The MIT300 dataset categories are highly varied and natural. The dataset can be used for model evaluation [Judd et al., 2012].



Fig. 7. MIT1003 and MIT300 datasets

**TORONTO** The TORONTO dataset included 120 chromatic images and was free-viewed by 20 subjects (see Fig.8). The datasets contained both outdoor and indoor scenes with a fixed resolution of  $511 \times 681$  pixels [Bruce and Tsotsos, 2005].



Fig. 8. TORONTO dataset

**SID4VAM** SID4VAM is a synthetic image database that is mainly used to psycho-physical evaluate the V1 properties (see Fig.9). The database is composed of 230 synthetic images. It includes 15 distinct types of low-level features (e.g., brightness, size, color, and orientation, etc.) with different a target-distractor pop-out type of synthetic images [Berga et al., 2019].

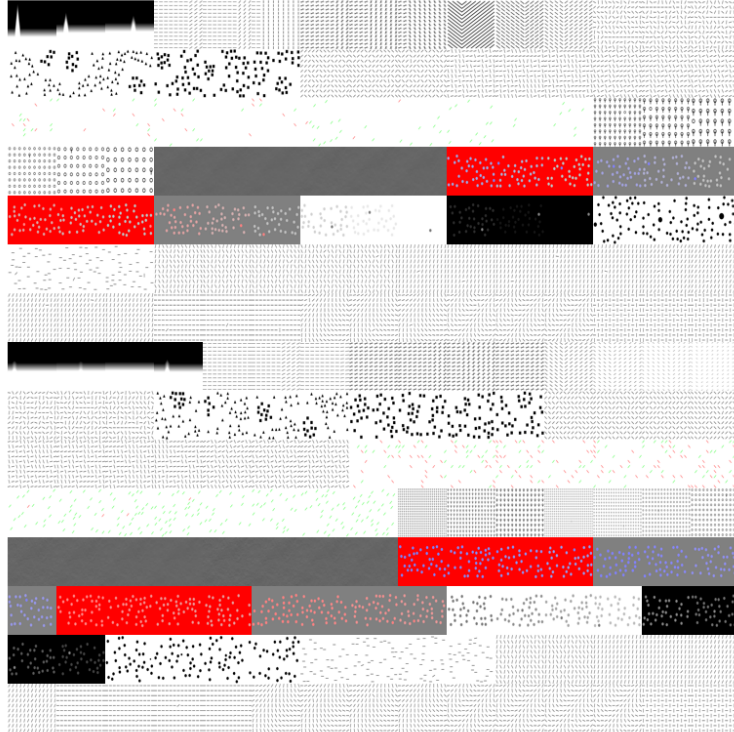


**Fig. 9.** SID4VAM dataset

### 3.2 Evaluation Metrics

There are several approaches, as we mentioned before, to evaluate metrics between visual saliency and model prediction. In general, saliency evaluation can be divided into two branches that location-based and distribution-based respective. The former mainly focuses on the district located in the saliency map, and the latter considers both predicted saliency and human eye fixation maps as continuous distributions. In this research, we used AUC, NSS, CC, SIM, IG, and KL as

evaluating methods, and details of each evaluate metric described as follows section.

**Area under ROC Curve (AUC)** The AUC-JUD metric is one of the popular approaches to evaluate saliency model performances. The saliency map can be treated as a binary classifier to split positive samples from negative samples by setting different thresholds. The actual positive (TP) is the saliency map values' proportion beyond a specific threshold at the fixation locations. In verse, false positive (FP) is the saliency map values' proportion beyond a specific threshold at the non fixation locations. In our case, the thresholds are set from the saliency map values [Borji et al., 2013].

**Normalized Scanpath Saliency (NSS)** The NSS metric usually measured the relationship between human eye fixation maps and model prediction saliency maps [Emami and Hoberock, 2013]. Given a binary fixation map  $F$  and saliency map  $S$ , The NSS can be formally defined as:

$$NSS = \frac{1}{N} \sum_{i=1}^N \bar{S}(i) x F(i) \quad (7)$$

Where,

$$N = \sum_i F(i) \text{ and } \bar{S} = \frac{S - \mu(s)}{\sigma(S)} \quad (8)$$

where  $N$  is the total number of human eye positions and  $\sigma(S)$  is the standard deviation.

**Similarity Metric (SIM)** The similarity metric (SIM) is a very famous algorithm from measure image structure similarity, and it has already widely used in image quality and image processing disciplines [Riche et al., 2013]. The SIM mainly measured the normalized probability distributions of eye fixation and model prediction saliency maps. The SIM can be mathematically described as:

$$SIM = \sum_{i=1} \min(P(i), Q(i)) \quad (9)$$

Where  $P(i)$  and  $Q(i)$  are the normalized saliency map and the fixation map, respectively. A similarity score should be located between zero and one.

**Information Gain (IG)** The information gain is an approach to measure saliency map prediction accuracy from the information-theoretic view. It mainly measured the critical information contained in the predict saliency map compared

with the ground truth map. The mathematical formula of IG can be expressed as:

$$IG(P, Q^B) = \frac{1}{N} \sum_i Q_i^B [\log_2(\epsilon + P_i) - \log_2(\epsilon + B_i)] \quad (10)$$

Where  $P$  indicate prediction saliency map, and  $Q^B$  is baseline map,  $\epsilon$  represents regularity parameters.

**Pearson’s Correlation Coefficient (CC)** Pearson’s Correlation Coefficient (CC) is one of the linear approaches that measured how many similarities between prediction saliency map and baseline map.

$$CC(P, Q^D) = \frac{\sigma(P, Q^D)}{\sigma(P) \times \sigma(Q^D)} \quad (11)$$

Where  $P$  indicates prediction saliency map and  $Q^D$  is the ground truth saliency map.

**Kullback-Leibler divergence (KL)** The Kullback-Leibler divergence (KL) was used to measure two distribution samples’ distance from information-theoretic views. It can be formally defined as:

$$KL(P, Q^D) = \sum_i Q_i^D \log\left(\epsilon + \frac{Q_i^D}{\epsilon + P_i}\right) \quad (12)$$

Where  $P$  indicates prediction saliency map and  $Q^D$  is the ground truth saliency map.  $\epsilon$  also represents regularity parameters.

## 4 Experimental Results

### 4.1 Quantitative Comparison of the Proposed Model with other State-of-the-Art Models

In order to evaluate the performance of the proposed model, we compared it to six state-of-the-art models. We selected MIT1003 and SID4VAM benchmarks for a comparison of the quantitative results. These results were reported in Table 1 and Table 2.

Models	NSS	SIM	AUC-Judd	IG	CC	KLD
ITII [Itti et al., 1998]	0.61	0.27	0.69	7.46	0.19	1.77
Achanta [Achanta et al., 2009]	0.18	0.21	0.55	5.71	0.05	2.98
AIM [Bruce and Tsotsos, 2005]	0.74	0.24	0.72	7.51	0.23	1.84
HFT [li et al., 2012]	1.34	0.38	0.82	8.14	0.42	1.30
ICL [Hou and Zhang, 2008]	1.12	0.36	0.79	7.31	0.35	1.87
SIM [Murray et al., 2011]	0.72	0.26	0.72	7.50	0.23	1.74
Proposed Model	0.88	0.32	0.74	4.90	0.28	3.54

**Table 1.** Quantitative scores of several models for the MIT1003 dataset. The red scores indicate best prediction model performance then follows with second (blue) and third (green) best prediction scores.

Models	NSS	SIM	AUC-Judd	IG	CC	KLD
ITII [Itti et al., 1998]	0.62	0.32	0.64	14.41	0.16	1.85
Achanta [Achanta et al., 2009]	0.29	0.11	0.52	-6.45	0.07	16.32
AIM [Bruce and Tsotsos, 2005]	0.43	0.24	0.57	-3.79	0.12	3.93
HFT [li et al., 2012]	2.13	0.46	0.77	14.81	0.54	1.59
ICL [Hou and Zhang, 2008]	1.11	0.39	0.74	14.42	0.34	1.86
SIM [Murray et al., 2011]	0.67	0.34	0.65	14.51	0.19	1.80
Proposed Model	0.67	0.33	0.64	7.63	0.19	6.56

**Table 2.** Quantitative scores of several models for the SID4VAM dataset. The red scores indicate best prediction model performance then follows with second (blue) and third (green) best prediction scores.

## 4.2 Qualitative Comparison of the Proposed Model with Other State-of-the-Art Models

We qualitatively tested the proposed model with the MIT1003, MIT300, TORONTO datasets (see Fig.10), and SID4VAM dataset, respectively. Meanwhile, we compared the model performance with other state-of-the-art saliency prediction modelings on the MIT1003 and SID4VAM datasets. Fig.11 and Fig.12 illustrate the saliency map results obtained when the proposed model and other state-of-the-art models are applied to sample images drawn from the studied dataset, and we can see that the proposed model can predict most of the salient objects in the given images. Furthermore, the proposed model can successfully detect the orientation, boundary, and pop out function when the model applied the SID4VAM dataset.

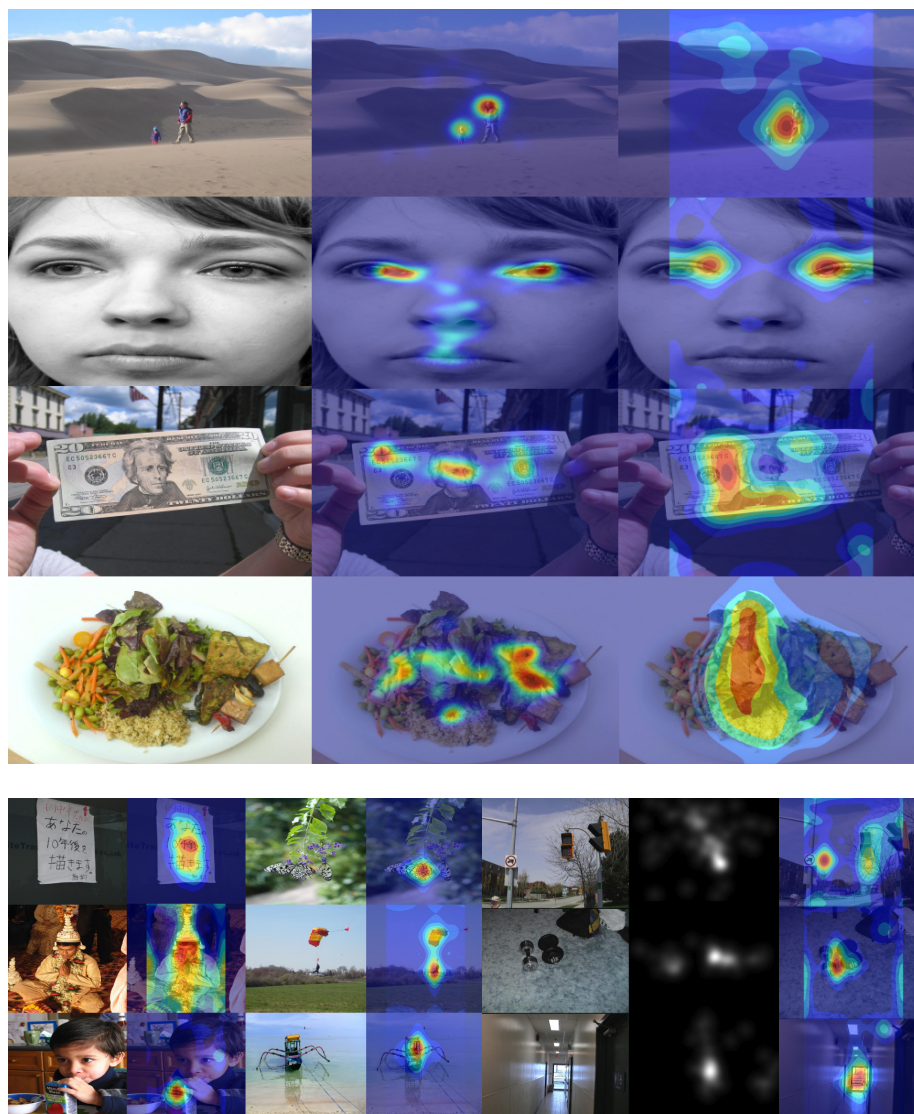


**Fig. 10.** Up: Performance evaluation with MIT1003 database. The first column is color images, second column is ground truth saliency map and the last column is proposed model prediction saliency map. Left: Performance evaluation with MIT300 database. The first and third column is color images. The second and fourth column is proposed model prediction saliency map. Right: Performance evaluation with TORONTO database. The first column is color images, second column is ground truth saliency map and the last column is proposed model prediction saliency map.

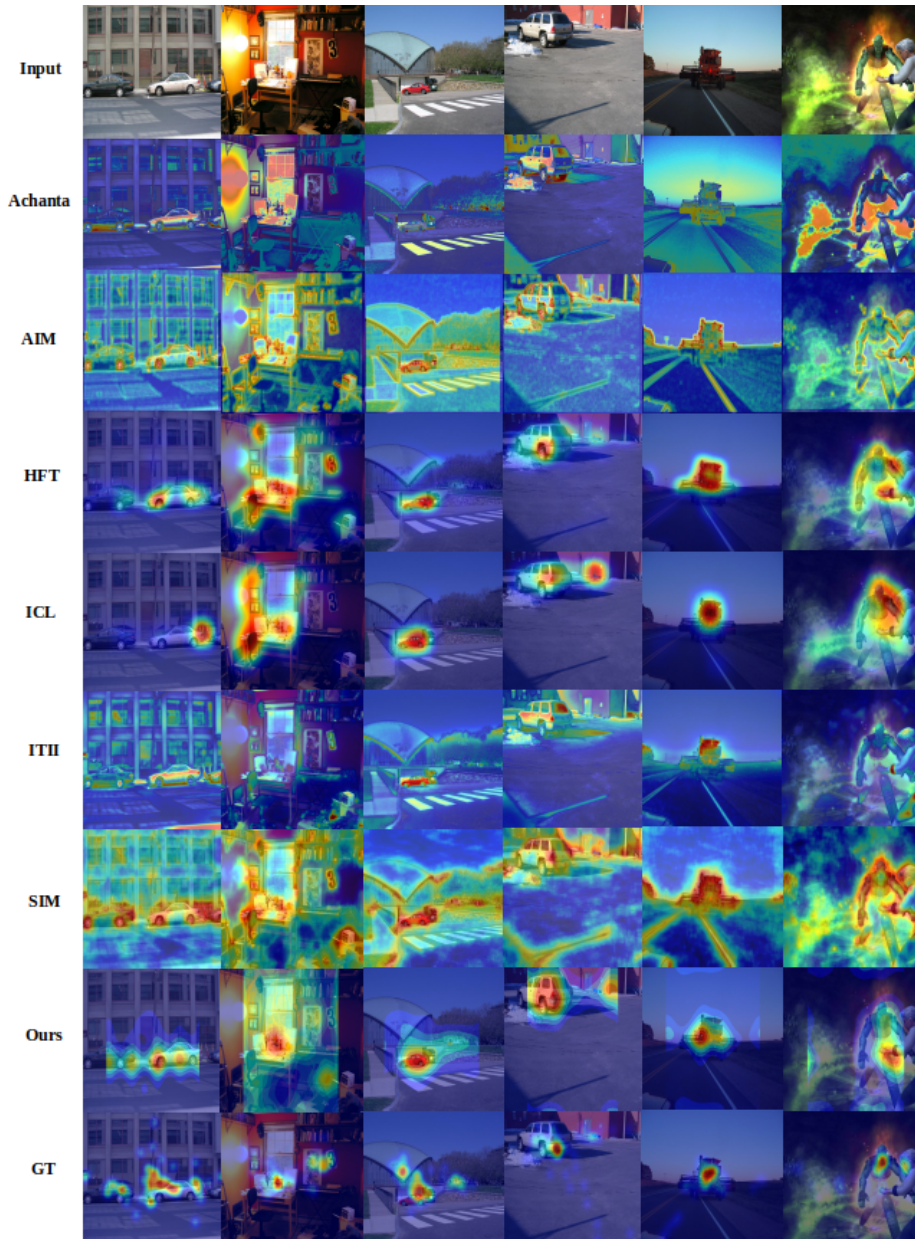


**Fig. 11.** Qualitative saliency prediction results with MIT1003 database with different models.

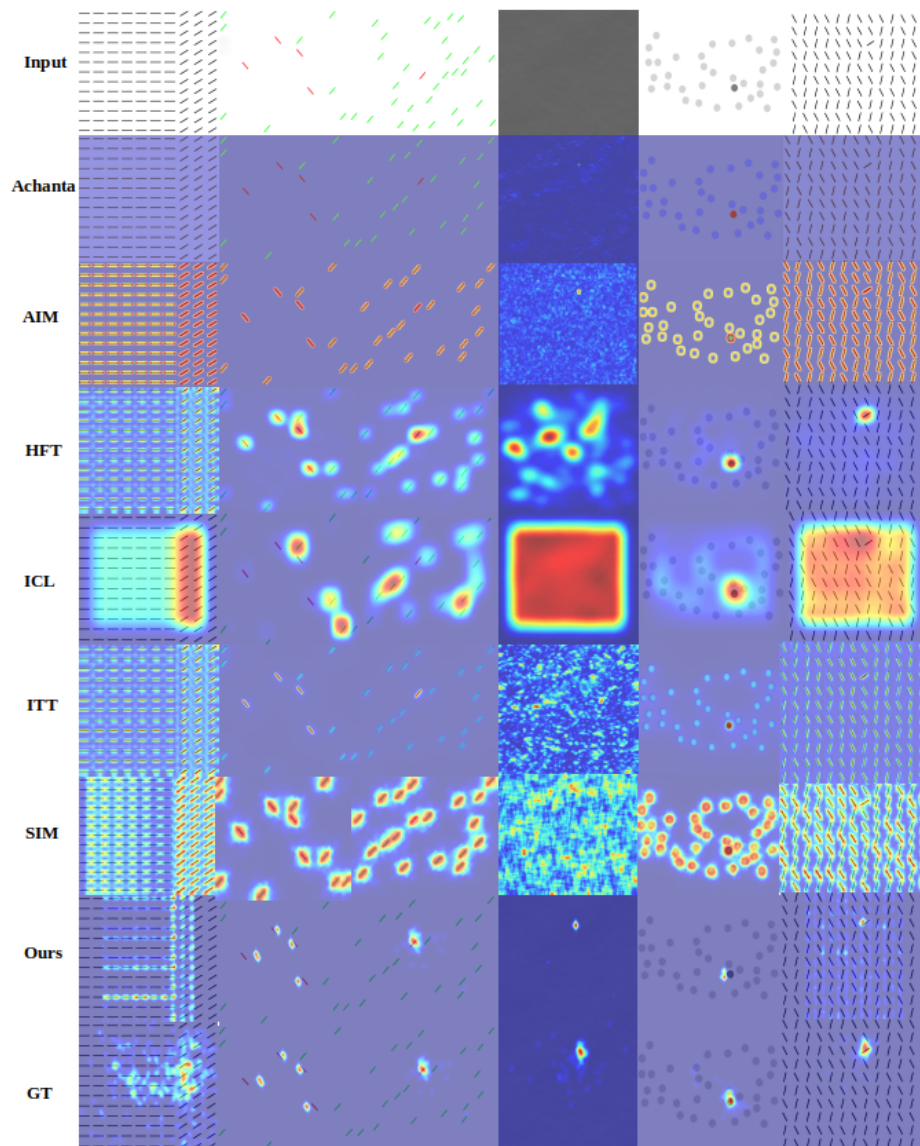


**Fig. 12.** Qualitative saliency prediction results with SID4VAM database with different models.

## 5 Conclusions

In this study, an HVS-Oriented computational visual saliency prediction modeling has been proposed, inspired by a low-level human visual pathway. This study uses color opponent channel, wavelet energy map, and contrast sensitivity functions to predict a saliency map. The model evaluates by three benchmark datasets and achieved slightly outperforms of visual saliency prediction. To my knowledge, this is the first time that combined wavelet energy map and contrasts sensitivity function to prediction saliency map, and I believe it can be transferred to video (spatial-temporal) saliency prediction in the future.

## 6 Code availability

Open-source software, written in Python, which performs all the experiments described in this article is available for download from <https://github.com/sinodanish/BioMulti-L-NL-Model/tree/master/saliency>.

## 7 Acknowledgments

This work was funded by the Generalitat Valenciana through the grant GrisoliaP/2019/035.

## 8 Conflicts of Interest

The authors declare no conflicts of interest.

## 9 abbreviations

HSV	Human Vision System
V1	Primary Visual Cortex
CNN	Convolution Neural Network
WT	Wavelet Transform
IWT	Inverse Wavelet Transform
AUC	Area under ROC curve
NSS	Normalized Scanpath Saliency
CC	Pearson's Correlation Coefficient
SIM	Similarity or histogram intersection
IG	InformationGain
KL	Kullback–Leibler divergence
CSF	Contrast Sensitivity Function
FT	Fourier Transform
DWT	Discrete Wavelet Transform
IDWT	Inverse Discrete Wavelet Transform
LGN	Lateral Geniculate Nucleus
GT	Ground Truth

## Bibliography

- R. Achanta, S. Hemami, F. Estrada, and S. Süsstrunk. Frequency-tuned salient region detection. *Proceedings of the IEEE Conference on Computer Vision Pattern Recognition (CVPR)*, 06 2009. <https://doi.org/10.1109/CVPR.2009.5206596>.
- H. Barlow. Sensory mechanisms, the reduction of redundancy, and intelligence. *Proc. of the Nat. Phys. Lab. Symposium on the Mechanization of Thought Process*, (10):535–539, 1959.
- H. Barlow. *Vision: Coding and Efficiency*, chapter A theory about the functional role and synaptic mechanism of visual aftereffects. Cambridge Univ. Press, Cambridge, UK, 1990.
- D. Berga, X. R. Fdez-Vidal, X. Otazu, and X. M. Pardo. Sid4vam: A benchmark dataset with synthetic images for visual attention modeling. *2019 IEEE/CVF International Conference on Computer Vision (ICCV)*, pages 8788–8797, 2019.
- A. Borji, H. Rezazadegan Tavakoli, D. Sihite, and L. Itti. Analysis of scores, datasets, and models in visual saliency prediction. pages 921–928, 12 2013. <https://doi.org/10.1109/ICCV.2013.118>.
- M. Brill. *Trichromatic Theory*, pages 827–829. 01 2014. ISBN 978-0-387-30771-8.
- N. Bruce and J. Tsotsos. Saliency based on information maximization. volume 18, 01 2005.
- S. Daly. The visible difference predictor: An algorithm for the assessment of image fidelity. 1992.
- M. Emami and L. Hoberock. Selection of a best metric and evaluation of bottom-up visual saliency models. *Image and Vision Computing*, 31:796–808, 10 2013. <https://doi.org/10.1016/j.imavis.2013.08.004>.
- U. Engelke, H. Liu, J. Wang, P. Le Callet, I. Heynderickx, H.-J. Zepernick, and A. Maeder. A comparative study of fixation density maps. *IEEE transactions on image processing : a publication of the IEEE Signal Processing Society*, 11 2012. <https://doi.org/10.1109/TIP.2012.2227767>.
- X. Hou and L. Zhang. Dynamic visual attention: Searching for coding length increments. volume 21, pages 681–688, 01 2008.
- L. Hurvich and D. Jameson. An opponent-process theory of color vision. *Psychological Review*, 64:384–404, 12 1957. <https://doi.org/10.1037/h0041403>.
- N. Imamoglu, W. Lin, and Y. Fang. A saliency detection model using low-level features based on wavelet transform. *IEEE Transactions on Multimedia*, 15: 96–105, 01 2013. <https://doi.org/10.1109/TMM.2012.2225034>.
- L. Itti. Models of bottom-up and top-down visual attention. 01 2000.
- L. Itti, C. Koch, and E. Niebur. A model of saliency-based visual attention for rapid scene analysis. *Pattern Analysis and Machine Intelligence, IEEE Transactions on*, 20:1254 – 1259, 12 1998. <https://doi.org/10.1109/34.730558>.
- T. Judd, F. Durand, and A. Torralba. A benchmark of computational models of saliency to predict human fixations. In *MIT Technical Report*, 2012.

- S. Kruthiventi, V. Gudisa, J. Dholakiya, and R. Babu. Saliency unified: A deep architecture for simultaneous eye fixation prediction and salient object segmentation. pages 5781–5790, 06 2016. <https://doi.org/10.1109/CVPR.2016.623>.
- M. Kümmerer, T. Wallis, and M. Bethge. Information-theoretic model comparison unifies saliency metrics. *Proceedings of the National Academy of Sciences*, 112: 201510393, 12 2015. <https://doi.org/10.1073/pnas.1510393112>.
- J. li, M. Levine, X. An, X. Xu, and H. He. Visual saliency based on scale-space analysis in the frequency domain. *IEEE Transactions on Pattern Analysis and Machine Intelligence*, 35:996–1010, 11 2012. <https://doi.org/10.1109/TPAMI.2012.147>.
- A. Louis, P. Maass, and A. Rieder. *Wavelets: Theory and Applications*. 01 1997. ISBN 978-0-471-96792-7.
- J. Mannos and D. Sakrison. The effects of a visual fidelity criterion of the encoding of images. *IEEE Transactions on Information Theory*, 20(4):525–536, 1974.
- K. Mullen. The contrast sensitivity of human color vision to red-green and blue-yellow chromatic gratings. *The Journal of physiology*, 359:381–400, 03 1985. <https://doi.org/10.1113/jphysiol.1985.sp015591>.
- N. Murray, M. Vanrell, X. Otazu, and C. A. Párraga. Saliency estimation using a non-parametric low-level vision model. pages 433–440, 06 2011. <https://doi.org/10.1109/CVPR.2011.5995506>.
- N. Riche, M. Duvinage, M. Mancas, B. Gosselin, and T. Dutoit. Saliency and human fixations: State-of-the-art and study of comparison metrics. 12 2013. <https://doi.org/10.1109/ICCV.2013.147>.
- A. Selvaraj and N. Shebiah. Object recognition using wavelet based salient points. *The Open Signal Processing Journal*, 2:14–20, 09 2009. <https://doi.org/10.2174/1876825300902010014>.
- R. Shapley and M. Hawken. Color in the cortex: Single- and double-opponent cells. *Vision research*, 51:701–17, 02 2011. <https://doi.org/10.1016/j.visres.2011.02.012>.
- Y. Sun and R. Fisher. Object-based visual attention for computer vision. *Artificial Intelligence*, 146:77–123, 05 2003. [https://doi.org/10.1016/S0004-3702\(02\)00399-5](https://doi.org/10.1016/S0004-3702(02)00399-5).
- A. Treisman and G. Gelade. A feature-integration theory of attention. *Cognitive psychology*, 12:97–136, 02 1980. [https://doi.org/10.1016/0010-0285\(80\)90005-5](https://doi.org/10.1016/0010-0285(80)90005-5).
- D. Wang, A. Kristjansson, and K. Nakayama. Efficient visual search without top-down or bottom-up guidance. *Perception & psychophysics*, 67:239–53, 03 2005. <https://doi.org/10.3758/BF03206488>.
- N. Wilming, T. Betz, T. Kietzmann, and P. König. Measures and limits of models of fixation selection. *PloS one*, 6:e24038, 09 2011. <https://doi.org/10.1371/journal.pone.0024038>.
- L. Zhaoping. A neural model of contour integration in the primary visual cortex. *Neural computation*, 10:903–40, 05 1998. <https://doi.org/10.1162/089976698300017557>.